1 A recombinant rotavirus harboring a spike protein with a heterologous peptide

2 reveals a novel role of VP4 in viroplasm stability

3 Guido Papa[a,*], Janine Vetter[b,1], Michael Seyffert[b], Kapila Gunasekera[c], Giuditta De Lorenzo[a,*],

4 Mahesa Wiesendanger[b,d], Elisabeth M. Schraner[b], Jean-Louis Reymond[c], Cornel Fraefel[b], Oscar R.

5 Burrone[a], Catherine Eichwald[b,#].

6

7 [a]Molecular Immunology Laboratory, International Centre for Genetic Engineering and

8 Biotechnology, Trieste, Italy

9 [b]Institute of Virology, University of Zurich, Zurich, Switzerland;

10 [c]Department of Chemistry and Biochemistry and Pharmaceutical Sciences, University of Bern,

11 Bern, Switzerland;

12 [d]Institute of Veterinary Anatomy, University of Zurich, Zurich, Switzerland.

13

14 Running Head: New role of rotavirus VP4

15

16 [#]**Address correspondence to** Catherine Eichwald, ceichwald@vetvir.uzh.ch

17 [1]**Author Contributions:** GP and JV contributed equally to this work.

18 ***Present address:** GP: MRC Laboratory of Molecular Biology, Cambridge, UK; and GDL: MRC-

19 University of Glasgow, Centre for Virus Research, Glasgow, UK

20 **Keywords:** rotavirus, spike-protein, viroplasm, VP4, reverse-genetics.

21

22 This manuscript has 230 words in the abstract and 5'232 words in the text.

23   **ABSTRACT**

24   The rotavirus (RV) VP4 spike protrudes as a trimeric structure from the five-fold axes of the

25   virion triple-layer. Infectious RV particles need to be proteolytically cleaved in VP4 into two

26   subunits, VP8* and VP5*, constituting both the distal part and central body of the virus spike.

27   Modification of VP4 has been challenging as it is involved in biological process including the

28   interaction with sialic acid and integrins, cell tropism and hemagglutinin activity. Here, we

29   engineered a loop at position K145-G150 in the lectin domain of the VP8* subunit to harbor a small

30   biotin acceptor peptide (BAP) tag and rescued viable viral particles using RV reverse genetics

31   system. This rRV/VP4-BAP internalizes, replicates, and generates virus progeny, demonstrating

32   that the VP4 spike of RV particles can be genetically manipulated by the incorporation of at least 15

33   exogenous amino acids. Although, VP4-BAP had a similar distribution as VP4 in infected cells by

34   localizing in the cytoskeleton and surrounding viroplasms. However, compared to wild-type RV,

35   rRV/VP4-BAP featured a reduced replication fitness and impaired viroplasm stability. Upon

36   treatment of viroplasms with 1,6-hexanediol, a drug disrupting liquid-liquid phase-separated

37   condensates, the kinetic of rRV/VP4-BAP viroplasm recovery was delayed, and their size and

38   numbers reduced when compared to viroplasms of wild type RV. Moreover, siRNA silencing of

39   VP4 expression in RV strain SA11 showed similar recovery patterns as rRV/VP4-BAP, revealing a

40   novel function of VP4 in viroplasm stability.

41   **IMPORTANCE** The rotavirus (RV) spike protein, VP4, has a relevant role in several steps

42   involving virion internalization. The strategic position of VP4 in the virion resulted in a challenge

43   for the addition of an exogenous peptide producing infectious particles. The identification of a

44   specific loop in position K145-G150 in the VP8* subunit of VP4 allowed the rescue by RV reverse

45   genetics of a recombinant RV harboring VP4 containing a 15 amino acids tag. This study

46   demonstrates this recombinant virus has similar replication properties as a wild-type virus.

47   Moreover, we also discovered that VP4 is necessary for the assembly and stabilization of the

48   cytosolic replication compartments, the viroplasms, demonstrating a novel role of this protein in the

49   RV life cycle.

50

51 **INTRODUCTION**

52   Rotavirus (RV) is the primary etiological agent responsible for severe gastroenteritis and

53 dehydration in infants and young children worldwide (1) as well as young animals such as piglets,

54 calves, and poultries, thus representing a negative economic impact on livestock (2-4). RV virions

55 are non-enveloped particles composed of three concentric layers. The virus core-shell encloses

56 eleven double-stranded RNA (dsRNA) genome segments and twelve copies of the structural

57 proteins VP1 (the RNA-dependent RNA polymerase) and the guanyl-methyltransferase VP3 (5, 6).

58 The icosahedral core-shell (T=1, symmetry) is composed of twelve decamers of VP2 and

59 surrounded by 260 trimers of the abundant structural protein VP6, constituting the transcriptionally

60 active double-layered particles (DLPs) (7, 8). On top of each VP6 trimer stands a trimer of the

61 glycoprotein VP7, the main building component of the outer layer of the virion that also shows an

62 icosahedral symmetry (T=13). At each of the 5-fold axes of the outer layer, the VP4 spike protein is

63 anchored in a trimeric conformation, although adopting a dimeric appearance when visualized from

64 the above capsid surface (9-12). Infectious RV virions, also named triple-layered particles (TLPs),

65 rely on the cleavage of the VP4 spike protein by a trypsin-like enzyme found in the intestinal tract

66 (13). The proteolytic cleavage of VP4 (88 kDa) entails two main products, VP8* (28 kDa, amino

67 acids 1-247) and VP5* (60 kDa, amino acids 248-776) that remain non-covalently associated with

68 the virion (14, 15). VP8* and a significant portion of VP5*, VP5CT (amino acids 246-477), as

69 analyzed by crystallography, constitute the distal globular density and the central body of the spike,

70 respectively (16, 17). The VP8* subunit has several functions such as haemagglutinin activity (18),

71 involvement in the binding to sialic acid (17), and a determinant role in virus tropism, while VP5*

72 has been implicated in the interaction with integrins (19-21). Interestingly, VP4 is not only involved

73 in RV tropism, attachment, neutralization, and entry into host cells, but has also been shown to play

74 an essential role in virion morphogenesis. During virus internalization, VP4 was shown to bind to

75 the small GTPase Rab5 and PRA1 within early endosomes (22), to directly activate the heat-shock

76   protein 70 (23, 24) and to bind to the actin-binding protein drebrin (25) followed by association to

77   the microtubules and actin cytoskeletons (26-31).

78   Specific *in vivo* biotinylation of cellular targets can be achieved by adding a small biotin

79   acceptor peptide tag (BAP) (15 amino acids) to the protein of interest and co-expressing with the

80   *Escherichia coli*-derived biotin ligase, BirA (32). This enzyme covalently links a single biotin

81   molecule to the unique lysine within the BAP tag (33, 34). This methodology is a powerful

82   biotechnological tool for versatile applications, such as identifying highly complex interactomes

83   (35, 36), and permits batch protein and subviral particle (33, 34) refinement at high purity and in

84   physiological conditions. An example is the incorporation of a BAP tag in RV VP6, allowing

85   preparation and purification of replication-competent DLPs (33).

86   Here, we describe the generation of a recombinant RV (rRV) harboring a genetically

87   modified genome segment 4 (gs4) encoding the structural protein VP4 with an in-frame inserted

88   BAP tag in an external loop of the VP8* subunit. The biotinylated rRV/VP4-BAP can infect,

89   replicate and generate virus progeny. Moreover, it revealed a novel function of VP4 associated to

90   viroplasm assembly and stability.

91   **RESULTS**

92   **Production and characterization of recombinant rotavirus expressing VP4-BAP protein.** As

93   VP4 is the main structural RV protein involved in host cell tropism, attachment, and internalization,

94   we addressed the question whether it could be engineered by incorporating a peptidic tag within its

95   coding sequence without compromising its structural and functional properties. To test this

96   hypothesis, we used the previously published crystal structure of simian RRV VP4 (10) to identify

97   four different loops localized in the lectin domain (amino acids 65-224) of the VP8* subunit and

98   then inserted a BAP tag (33, 34) in the corresponding loops of the simian strain SA11. As depicted

99   in **Fig. 1A,** the selected amino acid regions for the BAP tag insertions were T96-R101, E109-S114,

100   N132-Q137, and K145-G150 of VP4 of strain SA11, assigned with colors blue, orange, pink, and

101   green, respectively. The biotinylation of these BAP-tagged VP4 proteins was then analyzed in total

102   cell lysates in a Western blot-retardation assay (WB-ra) (34). Each of these constructs, driven by a

103   T7 promoter, was co-transfected with a DNA plasmid encoding the cytosolically localized enzyme

104   BirA (cyt-BirA) into MA104 cells, which were also infected with a recombinant T7 RNA

105   polymerase vaccinia virus to allow cytosolic transcription (37). It has been noticed that VP4 was

106   not expressed when transcribed using a nuclear promoter, probably due to mRNA splicing of the

107   VP4 transcript. As shown in **Fig. 1B**, the four VP4-BAP variants (**Fig. 1B, lanes 3-10**), but not the

108   wild type (wt) VP4 (**Fig. 1B, lanes 1 and 2**), were fully biotinylated. Of note, the band detected

109   above the VP4-BAP band corresponds to a phosphorylation form of the protein only present in

110   transfected cells but not in RV-infected cells, as demonstrated by the λ-phosphatase treatment (**Fig.**

111   **S1A and S1B**). Taken together, the results indicate that the expression and stability of the different

112   VP4 protein mutants were not affected by the location of the inserted BAP tag.

113   We next assessed whether these four VP4-BAP proteins could assemble into infectious

114   rotavirus particles and support virus replication. For this purpose, we took advantage of a newly

115   developed reverse genetics system to rescue recombinant rotavirus (rRV) harboring a genetically

116   modified genome segment 4 (gs4) encoding the different VP4-BAP proteins (gs4-BAP) (38-41).

117   We were able to rescue only the rRV harboring gs4-BAP encoding the BAP tag within the "green"

118   loop (**Fig. 1A and C**), herein named rRV/VP4-BAP, as demonstrated by the larger size of the

119   modified gs4-BAP compared to the wt gs4 in the dsRNA virus genome migration pattern (**Fig. 1C**)

120   and confirmed by Sanger sequencing (**Fig. S1C**). This outcome suggests that the "green" loop is the

121   only one that preserves virus infectivity when modified by the BAP tag. The rRV/VP4-BAP

122   replication kinetic was delayed compared to the recombinant wt strain (rRV/wt) (**Fig. 1D**), even

123   though similar viral titers were reached at 48 hours post-infection (hpi), suggesting that the VP4-

124   BAP integration in the virus particle affects the virus assembly rate.

125   We then investigated the ability of VP4-BAP produced by rRV/VP4-BAP to be biotinylated

126   in cells expressing the BirA enzyme. For this purpose, we generated MA104 cells stably expressing

127 cytosolic localized BirA (MA-cytBirA) and infected them with rRV/VP4-BAP. The produced VP4-

128 BAP protein showed biotinylation as demonstrated by a band of approx. 85 kDa detected after

129 incubation with StAv-peroxidase (**Fig.1E, lane 3**). As expected, VP4 biotinylation was detected

130 neither in rRV/wt infected MA-cytBirA cells (**Fig. 1E, lane 2**) nor in rRV/VP4-BAP infected

131 MA104 cells (**Fig. 1E, lanes 4, 5**). Using the WB-ra, we found that the fraction of biotinylated

132 VP4-BAP corresponded to 73% of the total protein (**Fig. 1F**).

133 We next examined if biotinylated VP4-BAP was able to be incorporated into newly

134 assembled virus particles. We therefore purified virions produced in MA-cytBirA cells in the

135 presence of biotin and estimated their biotinylation by the WB-ra. Consistent with our observation

136 in cell extracts, 67% of the VP4-BAP in virus particles was biotinylated (**Fig. 1G**). We additionally

137 visualized biotinylated VP4-BAP on purified virions by negative staining electron microscopy

138 followed by incubation with StAv conjugated to gold particles. Thus, the virions produced in the

139 presence of biotin were positive to the gold particles (53 %) (**Fig. 1H**). Interestingly, we also

140 identified the presence of virus coat-like layers by negative staining of purified rRV/VP4-BAP

141 particles (**Fig. S1D**) that were absent in samples of the purified rRV/wt, suggesting instability of the

142 rRV/VP4-BAP virions. Moreover, as shown in **Fig. S1E**, these particles appear to have a slightly

143 larger diameter (~80 nm) when compared to rRV/wt particles (~75 nm) but were still in the range of

144 TLPs (42).

145 **Internalization of rRV/VP4-BAP and cytosolic localization of VP4-BAP.** Since the virus

146 replication fitness of rRV/VP4-BAP was delayed compared to rRV-wt, we investigated whether this

147 was caused by a difference in virion internalization. Purified rRV/VP4-BAP and rRV/wt virions

148 labeled with StAv-Alexa 555 before infection were compared and analyzed for virus particle

149 internalization by CLSM. As a control, the virus particles were also immunostained with the

150 conformational monoclonal antibody (mAb) anti-VP7 (clone 159), which only recognizes the

151 trimeric form of the VP7 protein (43, 44). Initially (0 min), VP4-BAP and VP7 signals co-localized

152 on the cell surface, indicating association of virions to the cell membrane, while after two minutes

153   at 37ºC, both signals were found already internalized (**Fig. 2A**). These localization patterns were

154   comparable to the ones observed for the same time points with rRV/wt virions (anti-VP7, clone

155   159), suggesting no differences in the internalization mechanism between both viruses.

156   We then compared the localization of the newly produced biotinylated VP4-BAP in

157   rRV/VP4-BAP infected MA-cytBirA cells at 6 hpi, a time point with well-assembled viroplasms

158   (45). For this purpose, infected cells were incubated with or without biotin for 4 hours before

159   fixation. Biotinylated VP4-BAP, detected with StAv-Alexa 555, was found close to viroplasms

160   (revealed with anti-NSP5) and forming bundle-like structures presumably because of the

161   association of VP4 with microtubules and actin filaments (26, 29) (**Fig. 2B**). As expected, no StAv-

162   Alexa 555 signal was detected in cells infected with rRV/wt or with rRV/VP4-BAP in the absence

163   of biotin. Notably, the biotinylated VP4-BAP was found surrounding viroplasms and co-localizing

164   with VP7 in the endoplasmic reticulum (ER) (**Fig. 2C-D**), suggesting that the modification exerted

165   in VP4-BAP does not impact VP4 subcellular localization during RV replication.

166   **rRV/VP4-BAP revealed a role of VP4 in viroplasm stability.** We noticed a different behavior of

167   viroplasms formed by rRV/VP4-BAP or rRV/wt upon fixation of infected cells with methanol.

168   More precisely, few intact viroplasms were detectable in cells infected with rRV/VP4-BAP in

169   contrast to rRV/wt viroplasms, which remained as globular cytosolic inclusions (**Fig. S2A**).

170   Paraformaldehyde fixation did not show differences between the two viruses suggesting a

171   susceptibility of rRV/VP4-BAP viroplasms to alcohols. Since viroplasms have properties of liquid-

172   liquid phase-separated (LLPS) condensates (45-47), and rRV/VP4-BAP viroplasms are less stable,

173   we hypothesized that VP4 may have a yet unidentified role in the viroplasm stability. To challenge

174   this hypothesis, we used 1,6-hexanediol (1,6-HD), a well-described aliphatic alcohol able to disrupt

175   weak hydrophobic protein-protein or protein-RNA interactions, which are key drivers of liquid-

176   liquid phase separation (48, 49) and recently shown to be effective in dissolving RV viroplasms

177   (50). To visualize viroplasms formation in living cells, we took advantage of our previously

178   established MA104 cell line stably expressing NSP2 fused to the monomeric fluorescent protein

179   mCherry (herein named MA-NSP2-mCherry), which is recruited into viroplasms during RV

180   infection (40, 45, 46). Upon infection of MA-NSP2-mCherry cells with either rRV/VP4-BAP or

181   rRV/wt followed by addition of 1,6-HD for 6 min at 5 hpi (**Fig. 3A**), the viroplasms formed by both

182   rRVs dissolved and then readily recovered by 30 min after the compound was washed out (**Fig.**

183   **S2B**). Interestingly, the rRV-VP4-BAP viroplasms had a delayed recovery kinetic compared to

184   those from rRV/wt at short times after removing the drug (2 min) as denoted by quantifying either

185   the numbers of cells showing viroplasms (**Fig. 3B**) or the numbers of viroplasms per cell (**Fig. 3C**),

186   despite the reduced numbers of viroplasms present in cells infected with rRV-VP4-BAP (**Fig. 3D**)

187   just before the addition of 1,6 HD. Also, the initial size of rRV/VP4-BAP viroplasms was

188   significantly smaller than that of the rRV/wt viroplasms (**Fig. 3E**) and showed delayed size

189   recovery upon 1,6 HD removal (**Fig. 3F**). Notably, at 2 min post-recovery, the viroplasm

190   perinuclear localization was delayed as well for the virus with the tagged VP4 (**Fig. S2C-D**).

191   Next, we wanted to examine whether the liquid-like properties of rRV/VP4-BAP viroplasms

192   were altered. For this purpose, we measured the NSP2-mCherry diffusion dynamics in single

193   viroplasms using fluorescence recovery after photobleaching (FRAP) experiments (**Fig. 3G and**

194   **S2E**). Surprisingly, we found that the viroplasms fluorescence recovery after photobleaching at 5

195   hpi was similar for both viruses. Moreover, no differences were observed in the half-time recovery

196   or mobile fraction. (**Fig. S2F-G**). Thus, these results exclude differences in the liquid-like

197   properties of these globular inclusions. In order to further characterize the relationship between

198   viroplasms and VP4, we used a siRNA depletion approach. Although silencing of VP4 was

199   previously shown to impair assembly of the virion-third layer leading to the accumulation of DLPs,

200   viroplasms were still formed (**Fig. S3A-B**) (51). We thus reasoned that in the absence of VP4,

201   viroplasms should have similar behavior as those observed during rRV/VP4-BAP infection.

202   Although methanol fixation of viroplasms in VP4 silenced cells and infected with RV strain SA11

203   did not substantially affect viroplasm morphology to the same extend as that of rRV/VP4-BAP

204   (**Fig. S3C**). Specifically, the viroplasms in the cells infected with the wt virus showed a diffuse

205 morphology while those in rRV/VP4-BAP completely dissolved. As described above, experiments

206 performed with 1,6-HD (**Fig. S3D**) had a similar delayed viroplasm recovery kinetic on VP4-less

207 viroplasms as observed for rRV/VP4-BAP viroplasms **(Fig. 3H). Moreover,** the number (**Fig. 3I**)

208 and the size (**Fig. 3J**) of viroplasms were both decreased in siVP4 treated cells when compared to

209 the experimental controls.

210   Collectively, our data indicate that VP4 can be modified by the insertion of relatively short

211 tags at least in one position within the VP8* lectin domain of VP4 and suggest that VP4 plays a role

212 in the stability and dynamics of the viroplasms.

213 **DISCUSSION**

214   The external coat layer of the RV virion can be modified by adding *in vitro* a specific ratio

215 of VP7 and VP4 proteins to purified DLPs to generate recoated TLPs (rcTLPs) (10-12, 52), which

216 is a valuable tool to study the VP4 structural requirements allowing virion internalization (10).

217 However, rcTLPs have methodological limitations and do not allow transferring the parental

218 phenotype to the virus progeny. Moreover, rcTLPs only allow single amino acid substitutions of the

219 spike VP4 (53, 54). Here, we used a RV reverse genetics system (40) to show that it is possible to

220 modify an RV structural protein and specifically to remodel the spike protein VP4. For this purpose,

221 four exposed loops present in the VP8* subunit lectin domain were modified by incorporating a

222 short BAP tag of 15 amino acids. Interestingly, although the four differently modified proteins

223 could be efficiently biotinylated in transfected cells, only one of them, with a BAP tag inserted in

224 the K145-G150 loop, could be incorporated into infectious viral particles and rescued by reverse

225 genetics. The addition of BAP tags in other positions of the VP8* subunit may destabilize the VP4

226 structure, interfering with its incorporation into the virion and, thus, not allowing the rescue of

227 infectious viruses. We reasoned, therefore, that these VP4-BAP versions are strongly compromise

228 newly generated virions because they might directly impact: *i)* the transition from upright

229 (immature) to reverse (mature) conformational VP4 states (53); *ii)* the association with specific

230 cellular receptors (19, 20) or, *iii)* the incorporation of VP4 in the coat layer.

231   The internalization of RV virions requires a sequence of events involving interaction with

232 the cell- membrane, followed by invagination, and then engulfment into endosomes. This process

233 triggers a decrease of calcium levels within the endosomes, which induces loss of the virion VP4-

234 VP7 outer layer and the release of transcriptionally active DLPs into the cytosol (54-57). The

235 internalization kinetics of the rRV/VP4-BAP, as denoted by the ability to reach the cytosol, were

236 found to be comparable to that of the rRV/wt. Also, VP4-BAP and VP4 share similar distribution

237 patterns in infected cells, such as localization surrounding viroplasms, co-localization in the

238 endoplasmic reticulum with VP7, and incorporation into newly assembled virions. However, we

239 found that rRV/VP4-BAP has a reduced virus replication fitness compared to rRV/wt. Intriguingly,

240 rRV/VP4-BAP viroplasms seemed to be less resistant to methanol fixation than rRV/wt, which led

241 us to analyze viroplasms in the context of LLPS condensates by using the well-described 1,6-HD

242 (48, 49), which compromises RV viroplasms integrity. Upon 1,6-HD removal, the re-assembly of

243 rRV/VP4-BAP viroplasms was slower, and their number and size were reduced compared to

244 rRV/wt. However, no differences in viroplasm liquid-like dynamics were found when the mobility

245 of NSP2-mCherry was analyzed on single-viroplasm FRAP experiments, suggesting that the

246 reduction observed for rRV/VP4-BAP was related to a flawed process in the viroplasm assembly

247 but not to already formed inclusions. Our results are consistent with viroplasm behavior as LLPS

248 condensates(50). The only difference between rRV/VP4-BAP and the rRV/wt resides in the

249 structure of VP4, implying a role of VP4 in the structural stability of viroplasms. On this line of

250 thinking, the rRV/VP4-BAP viroplasms behavior was further confirmed by silencing VP4 in SA11-

251 infected cells. Consistent with a previous publication (51), the viroplasm formation was not affected

252 by the depletion of VP4. Nevertheless, the effect on viroplasm recovery kinetic after 1,6-HD

253 treatment was similar to the one observed on rRV/VP4-BAP viroplasms. Altogether, our data

254 support a new functional role of VP4 directly linked to the stabilization and assembly of

255   viroplasms. In fact, VP4 has been described to interact with the actin cytoskeleton and the RV

256   restrictive factor drebrin (25, 29, 30). Interestingly, a highly conserved actin-binding domain

257   present in the C-terminus of VP4 has been shown to remodel actin bundles to favor RV exit (27,

258   28). Most of these VP4-cytoskeleton associations involve the VP5* subunit. Intriguingly, since the

259   alteration of viroplasm stability was observed upon modification of the VP8* subunit, we

260   hypothesize that the VP8* subunit is involved in at least one of these three aspects that render the

261   viroplasms assembled and stabilized: *i)* association of VP8* with a yet undescribed host

262   component, *ii)* a reorganization ofVP5*-VP8* association or *iii)* a direct role of VP8* over another

263   RV protein(s).

264   Identifying a target site in the spike VP4 (loop region K145-G150) permissive for the

265   insertion of an exogenous peptide may impact the RV field. This VP4 modification favors the

266   insertion of peptides required for super-resolution microscopy or DNA-paint technologies (e.g.,

267   Halo or BC2 tags) to dissect debated aspects of RV entry. In addition, this VP4 modification

268   technology could permit the incorporation of antigenic peptides for vaccine development. Although

269   it is well-known that the current oral RV vaccines elicit an immune response (58, 59), the use of

270   rRV harboring a modified VP4 could provide an improved vaccination platform for the display of

271   other antigens fostering the development of a new generation of dual-vaccines.

272   **MATERIALS AND METHODS**

273   **Cells and viruses.** MA104 cells (embryonic African green monkey kidney cells; ATCC CRL-2378)

274   were grown in Dulbecco's modified Eagle's medium (DMEM) (Life Technologies) containing 10%

275   fetal calf serum (FCS) (AMIMED; BioConcept, Switzerland) and penicillin (100 U/ml)–

276   streptomycin (100 μg/ml) (Gibco, Life Technologies). MA/cytBirA and MA/NSP2-mCherry (40)

277   cell lines were grown in DMEM supplemented with 10% FCS, penicillin (100 U/ml)-streptomycin

278   (100μg/ml) and 5μg/ml puromycin (InvivoGen, France). BHK-T7/9 (baby hamster kidney stably

279   expressing T7 RNA polymerase) cells were kindly provided by Naoto Ito (Gifu University,

280 Japan)(60) and cultured in Glasgow medium supplemented with 5% FCS, 10% tryptose phosphate

281 broth (Sigma-Aldrich), 10% FCS, penicillin(100 U/ml)-streptomycin (100μg/ml), 2% nonessential

282 amino acids and 1% glutamine.

283 rRV/wt (40), rRV/VP4-BAP, and simian rotavirus strain SA11 (G3P6[1])(61) were

284 propagated, grown, and purified as previously described (62). Virus titer was determined as

285 viroplasm forming units per ml (VFU/ml) as described by (45). The T_7 RNA polymerase

286 recombinant vaccinia virus (strain vvT7.3) was amplified as previously described (37).

287 **Cell line generation.** MA/cyt-BirA cell line was generated using the PiggyBac technology (63).

288 Briefly, 10^5 MA104 cells were transfected with the pCMV-HyPBase (63) and transposon plasmids

289 pPB-cytBirA using a ratio of 1:2.5 with Lipofectamine 3000 (Sigma-Aldrich) according to the

290 manufacturer's instructions. The cells were maintained in DMEM supplemented with 10% FCS for

291 three days and then incubated with DMEM supplemented with 10% FCS and 5 μg/ml puromycin

292 (Sigma-Aldrich) for four days to allow the selection of cells expressing the gene of interest (40).

293 **Reverse genetics**. rRV/VP4-BAP was prepared as described previously (40, 41) using a pT$_7$-VP4-

294 BAP instead of pT$_7$-VP4. Briefly, monolayers of BHK-T$_7$ cells (4×10^5) cultured in 12-well plates

295 were co-transfected using 2.5 μL of TransIT-LT1 transfection reagent (Mirus) per microgram of

296 DNA plasmid. The mixture comprised 0.8 μg of SA11 rescue plasmids: pT$_7$-VP1, pT$_7$-VP2, pT$_7$-

297 VP3, pT$_7$-VP4-BAP, pT$_7$-VP6, pT$_7$-VP7, pT$_7$-NSP1, pT$_7$-NSP3, pT$_7$-NSP4, and 2.4 μg of pT$_7$-

298 NSP2 and pT$_7$-NSP5 (38, 39). Additionally, 0.8 μg of pcDNA3-NSP2 and 0.8 μg of pcDNA3-

299 NSP5, encoding NSP2 and NSP5 proteins, were co-transfected to increase rescue efficiency (40,

300 41). Cells were co-cultured with MA104 cells for three days in serum-free DMEM supplemented

301 with trypsin from porcine pancreas (0.5 μg/ml final concentration) (T0303-Sigma Aldrich) and

302 lysed by freeze-thawing. 300 μL of the lysate was transferred to fresh MA104 cells and cultured at

303 37°C for four days in serum-free DMEM supplemented with 0.5 μg/ml trypsin until a visible

304 cytopathic effect. The modified genome segments of rescued recombinant rotaviruses were

305 confirmed by specific PCR segment amplification followed by sequencing (40).

306   **Antibodies and Chemicals.** Guinea pig anti-NSP5, guinea pig anti-RV, and rabbit anti-VP4 were

307   described previously (45, 64, 65). Rabbit anti-NSP3 was kindly provided by Susana Lopez

308   (UNAM, Mexico), Mouse monoclonal anti-VP7 (clone 159) was kindly provided by Harry

309   Greenberg (Stanford University, CA, USA). Mouse mAb anti-glyceraldehyde dehydrogenase

310   (GAPDH) (clone GAPDH-71.1) and mouse anti-alpha tubulin (clone B-5-1-12) were purchase to

311   Merck. Streptavidin-HRP was purchased from Merck. Streptavidin-Alexa 555 and secondary

312   antibodies conjugated to Alexa 488, Alexa 594, Alexa 647, Alexa 700 (ThermoFisher Scientific).

313   **DNA plasmids.** pcDNA-VP4-SA11 was obtained by RT-PCR amplification of VP4 ORF of gs 4

314   from rotavirus simian strain SA11 (66) using specific primers to insert *Hind*III and *Xho*I sites,

315   followed by ligation into those sites in pcDNA3 (Invitrogen). pcDNA-VP4-*Kpn*I/*BamH*I was built

316   by insertion of point mutations in pcDNA-VP4-SA11 using the QuikChange site-directed

317   mutagenesis kit and protocol (Agilent) to insert *Kpn*I and *BamH*I restriction sites in VP4. pcDNA-

318   VP4-BAP (blue), (orange), (pink), and (green) were obtained by ligation between *Kpn*I and *BamH*I

319   of pcDNA-VP4-*Kpn*I/*BamH*I a synthetic DNA fragment (GenScript®) containing BAP tag in VP4

320   loops in amino acid regions 96-101, 109-114, 132-137 and 145-150, respectively. The BAP tags are

321   flanked by *BspE*I and *Nhe*I restriction sites for easy tag replacement. A detailed list of used DNA

322   sequence fragments is in *SI Appendix, Table 1*.

323   RV plasmids pT_7-VP1-SA11, pT_7-VP2-SA11, pT_7-VP3-SA11, pT_7-VP4-SA11, pT_7-VP6-

324   SA11, pT_7-VP7-SA11, pT_7-NSP1-SA11, pT_7-NSP2-SA11, pT_7-NSP3-SA11, pT_7-NSP4-SA11, and

325   pT_7-NSP5-SA11 were previously described (38). pcDNA3-NSP5 and pcDNA3-NSP2 were already

326   described (40). pT_7-VP4-BAP (blue), (orange), (green), and (pink) were obtained by inserting a

327   synthetic DNA fragment (Genscript) encoding for the VP4 protein-encoding BAP tag flanked by

328   *Mfe*I and *Nde*I restriction enzymes sites and ligated into those sites in the pT_7-VP4-SA11. A list of

329   the synthesized DNA fragment is *SI Appendix, Table 1*.

330   pPB-cytBirA plasmid was obtained from a synthetic DNA fragment (Genscript) containing

331   the BirA enzyme open reading frame of *Escherichia coli* (UniProt accession number: P06709) and

332   inserted in the pPB-MCS vector (41) using *Nhe*I-*BamH*I restriction enzymes sites.

333   **Streptavidin-supershift assay.** The assay was performed as described by Predonzani et al.(34).

334   Briefly, cell extracts were lysed in TNN lysis buffer (100mM Tri-HCl pH8.0, 250 mM NaCl, 0.5%

335   NP-40, and cOmplete protease inhibitor (Roche)) and centrifuged for 7 min at 15'000 rpm and 4˚C.

336   The supernatant was exhaustively dialyzed against PBS (phosphate-buffered saline, 137 mM NaCl,

337   2.7 mM KCl, 8 mM Na_2HPO_4, and 2 mM KH_2PO_4 pH 7.2) at 4˚C and heated for 5 min at 95˚C in

338   Laemmli sample buffer. Samples were incubated for 1 h at 4˚C with 1 μg streptavidin (Sigma) and

339   then resolved in SDS-polyacrylamide gel under reducing conditions. Proteins were transferred to

340   nitrocellulose 0.45 μm (67) and incubated with corresponding primary and secondary antibodies.

341   Secondary antibodies were conjugated to IRDye680RD or IRDye800RD (LI-COR, Germany) for

342   protein detection and quantification in Odyssey® Fc (LI-COR Biosciences).

343   **Virus fitness curve.** The experiment was performed as described previously (47) with some

344   modifications. MA104 cells (2×10^5) seeded in 12-well plates were infected with rRV at an MOI of

345   10 VFU/cell. The virus was allowed to adsorb for 1 h at 4°C, followed by incubation at 37°C in 500

346   μl DMEM. At the indicated time points, the plates were frozen at −80°C. The cells were then

347   treated with three freeze-thaw cycles, harvested, and centrifuged at $17,000 \times g$ for 5 min at 4°C.

348   The supernatant was recovered and activated with 80 μg/ml of trypsin for 30 min at 37°C. Two-fold

349   serial dilutions were prepared and used to determine the viral titers described previously (40, 41).

350   **Fluorescence labeling of purified rRV**. 100 μl of purified biotinylated rRV/VP4-BAP is activated

351   for 30 min at 37°C with 4 ul trypsin (2 mg/ml). The mixture is then incubated with 1 μl of

352   streptavidin-Alexa Fluor 555 (2mg/ml) (ThermoFisher Scientific) for 1 h at room temperature. The

353   tube was snaped every 20 min. Unbound streptavidin was separated labeled virus by loading the 50

354   μl reaction mixture on top of 100 μl of a 20% sucrose-PBS cushion. Samples were centrifuged for

355   40 min at 20 psi on Airfuge air-driven ultracentrifuge (Beckman Coulter). Pellet was resuspended in

356   20 µl Tris-buffered saline (TBS) buffer (25 mM Tris-HCl, pH 7.4, 137 mM NaCl, 5 mM KCl, 1

357   mM MgCl$_2$, 0.7 mM CaCl$_2$, 0.7 mM Na$_2$HPO$_4$, 5.5 mM dextrose).

358   **Immunofluorescence.** For virus internalization experiments, 1 µl of rRV particles conjugated to

359   SA-Alexa555 diluted in 50 µl of DMEM was adsorbed over MA104 cells for 15 min in a metal tray

360   cooled to -20°C. Cells were then transferred to 37°C and fixed at the indicated time-points with ice-

361   cold methanol for 3 min on dry ice.

362   For later times post-infection, the virus was adsorbed for 1h at 4°C in a reduced volume.

363   Then, cells were transferred to 37°C, treated at the indicated time points with 100µM biotin in

364   DMEM serum-free. Cells were fixed in 2% paraformaldehyde in phosphate-buffered saline (PBS)

365   for 10 min at room temperature. All immunofluorescences were processed as described by

366   Buttafuoco *et al.* (67). Images were acquired using a confocal laser scanning microscope (CLSM)

367   (DM550Q; Leica). Data were analyzed with the Leica Application Suite (Mannheim, Germany) and

368   Image J (68).

369   **LLPS characterization.** MA/NSP2-mCherry cells were seeded at a density of 1.2×10^4 cells per

370   well 8-wells Lab-Tek® Chamber Slide™ (Nunc, Inc. Cat #177402). For RV infection, the virus was

371   adsorbed at MOI of 25 VFU/cell diluted in 30 µl of DMEM serum-free, incubated at 4°C for 1 h in

372   an orbital shaker and then volume filled to 100µl with DMEM-serum-free followed by incubation at

373   37°C. At 5 hpi, the media was replaced by media containing 3.5% 1,6-hexanediol (Sigma-Aldrich)

374   in 2% FCS-DMEM and cells were incubated for 6 min at 37°C. Then the drug was washed out by

375   removing the media, washing the cells three times with PBS, and adding fresh 2%FCS-DMEM and

376   incubated at 37°C. At designated time post-recovery, cells were fixed with 2% PFA for 10 min at

377   room temperature. Nuclei were stained by incubating cells with 1 µg/ml of DAPI (4',6-diamidino-2-

378   phenylindole) in PBS for 15 min at room temperature. Samples were mounted in ProLong™ Gold

379   antifade mountant (Thermo Fischer Scientific), and Images were acquired using a fluorescence

380   microscope (DMI6000B, Leica). Data were analyzed with ImageJ (version 2.1.0/1.53;

381   https://imagej.net/Fiji).

382   **Quantification of viroplasms.** Number, size, and perinuclear localization of viroplasms were

383   essentially acquired and analyzed as previously described (45, 69-71). The viroplasm perinuclear

384   ratio was determined as previously described (69, 70) using the following formula: (V-N)/N,

385   whereas V, area occupied by viroplasm and N, area of the nucleus. Data analysis was performed

386   using Microsoft® Excel (version 16.46), and the statistical significance of differences was

387   determined by unpaired parametric Welch's t-test comparison post-test, using Prism 9 (GraphPad

388   Software, LLC).

389   **Rotavirus genome pattern visualization**. Rotavirus genome extraction and visualization were

390   performed as previously described (40, 41).

391   **Negative staining of purified particles.** For staining of biotinylated TLPs with streptavidin-gold,

392   purified particles were dialyzed overnight at 4°C in TNC buffer (10 mM Tris-HCl, pH 7.5, 140 mM

393   NaCl, 10mM $CaCl_2$). The TLPs were adsorbed for 10 min on carbon-coated Parlodion films

394   mounted on 300-mesh copper grids (EMS). Samples were washed once with water, fixed in 2.5%

395   glutaraldehyde in 100 mM Na/K-phosphate buffer, pH 7.0, for 10 min at room temperature, and

396   washed twice with PBS before incubation with 10 µl streptavidin conjugated to 10 nm colloidal

397   gold (Sigma-Aldrich, Inc) for 2 h at room temperature. The streptavidin-gold conjugated was

398   treated as described previously (63) before use to separate unconjugated streptavidin from

399   streptavidin-conjugated (72) to colloidal gold. The viral particles were further washed three times

400   with water and stained with 2% phosphotungstate, pH 7.0 for 1 min at room temperature. Samples

401   were analyzed in a transmission electron microscope (CM12; Philips, Eindhoven, The Netherlands)

402   equipped with coupled device (CCD) cameras (Ultrascan 1000 and Orius SC1000A; Gatan,

403   Pleasanton, CA, USA) at an acceleration voltage of 100 kV.

404   For calculation of the diameter of virus particles by negative staining, the area of each virus

405   particle was calculated using Imaris software (version 2.1.0/1.53c; Creative Commons license) and

406   then converted to the diameter as follow: π, where a is the area and d is the diameter of the particle,

407   respectively.

408 **siRNA reverse transfection.** For silencing gs 4 of SA11strain, the following siRNA pool: siVP4-

409 25 (5'-UUGCUCACGAAUUCUUAUAUATT-3'), siVP4-931(5'-GAAGUUACCGCACAUACUAUATT-

410 3') and siVP4-1534 (5'-AUUGCAAUGUCGCAGUUAAUATT -3' pool was designed and synthesized

411 by Microsynth AG (Switzerland). siRNA-A (sc-37007, Santa Cruz Biotechnology) was used as

412 scrambled siRNA. siRNA reverse transfection was performed by mixing 1.2 µl siRNA 5 µM with 1

413 µl lipofectamine RNAiMAX transfection reagent (Invitrogen, ThermoFisher Scientific) to a final

414 volume of 100 µl with Opti-MEM® (Gibco, ThermoFisher Scientific) in a well of 24-well plate and

415 incubated for 20 min at room temperature. To reach a 10nM siRNA final concentration, 2×10^4 cells

416 diluted in 500 µl DMEM supplemented with 10% FCS are added on top and incubated for 60 h

417 previous to analysis. Thus, cells were infected with RV strain SA11 at MOI 12 VFU/cell as

418 described previously (45, 47, 67).

419 **FRAP.** 1.2×10^4 MA/NSP2 cells per well were seeded in µ-Slide 18-well glass-bottom plates

420 (Ibidi). Cells were RV-infected at MOI of 15 VFU/cell and kept in DMEM-SF. At 4.5 hpi, the cells

421 were counterstained with Hoechst 33342 diluted in FluoroBRITE DMEM (Gibco, Cat.No. A18967-

422 01) at a concentration of 1µg/ml, incubated for 30 min at 37°C and subjected to FRAP analysis.

423 FRAP experiments were performed with an SP8 Falcon confocal laser scanning microscope

424 (CLSM) from Leica equipped with a 63x objective (NA 1.4) using the FRAP function of the LasX

425 software (Leica) as follows: a circular area of 2 µm in diameter, encompassing an entire viroplasm,

426 was bleached with the 405 nm and 481 nm lasers at 100% laser power for 20 iterations. The

427 fluorescent recovery was monitored by taking fluorescence images of the mCherry channel every 2

428 seconds for 140 min. For each FRAP acquisition, a circular area of 2 µm, encompassing an entire

429 unbleached viroplasm in the same cell, was used as the fluorescent control, and a squared area of 5

430 µm x 5 µm was chosen as background. The entire FRAP dataset was analyzed with MatLab

431 (MATLAB R2020b, Mathworks) using the FRAP-tool source code from easyFRAP (Cell Cycle

432 Lab, Medical School, University of Patras). Fully normalized data were used to generate FRAP

433   diagrams and calculate recovery half-times (T-half) and mobile fractions from independent

434   measurements. Representative images were taken and processed for each FRAP experiment using

435   the Imaris software v9.5 (Bitplane, Oxford Instruments). Fluorescent intensities of FRAP movies

436   were normalized using a customized Fiji pipeline (68).

442   **REFERENCES**

443   1.   Troeger C, Khalil IA, Rao PC, Cao S, Blacker BF, Ahmed T, Armah G, Bines JE, Brewer
444   TG, Colombara DV, Kang G, Kirkpatrick BD, Kirkwood CD, Mwenda JM, Parashar UD,
445   Petri WA, Riddle MS, Steele AD, Thompson RL, Walson JL, Sanders JW, Mokdad AH,
446   Murray CJL, Hay SI, Reiner RC. 2018. Rotavirus vaccination and the global burden of
447   rotavirus diarrhea among children younger than 5 years. JAMA Pediatr 172:958-965.
448   2.   Gomez DE, Weese JS. 2017. Viral enteritis in calves. Can Vet J 58:1267-1274.
449   3.   Vlasova AN, Amimo JO, Saif LJ. 2017. Porcine rotaviruses: epidemiology, immune
450   responses and control strategies. Viruses 9: 48.
451   4.   Dhama K, Saminathan M, Karthik K, Tiwari R, Shabbir MZ, Kumar N, Malik YS, Singh
452   RK. 2015. Avian rotavirus enteritis - an updated review. Vet Q 35:142-58.
453   5.   Lawton JA, Zeng CQ, Mukherjee SK, Cohen J, Estes MK, Prasad BV. 1997. Three-
454   dimensional structural analysis of recombinant rotavirus-like particles with intact and
455   amino-terminal-deleted VP2: implications for the architecture of the VP2 capsid layer. J
456   Virol 71:7353-60.
457   6.   Zhang X, Settembre E, Xu C, Dormitzer PR, Bellamy R, Harrison SC, Grigorieff N. 2008.
458   Near-atomic resolution using electron cryomicroscopy and single-particle reconstruction.
459   Proc Natl Acad Sci U S A 105:1867-72.
460   7.   Charpilienne A, Lepault J, Rey F, Cohen J. 2002. Identification of rotavirus VP6 residues
461   located at the interface with VP2 that are essential for capsid assembly and transcriptase
462   activity. J Virol 76:7822-31.
463   8.   Lepault J, Petitpas I, Erk I, Navaza J, Bigot D, Dona M, Vachette P, Cohen J, Rey FA. 2001.
464   Structural polymorphism of the major capsid protein of rotavirus. EMBO J 20:1498-507.
465   9.   Li Z, Baker ML, Jiang W, Estes MK, Prasad BV. 2009. Rotavirus architecture at
466   subnanometer resolution. J Virol 83:1754-66.
467   10.   Settembre EC, Chen JZ, Dormitzer PR, Grigorieff N, Harrison SC. 2011. Atomic model of
468   an infectious rotavirus particle. EMBO J 30:408-16.
469   11.   Yoder JD, Dormitzer PR. 2006. Alternative intermolecular contacts underlie the rotavirus
470   VP5* two- to three-fold rearrangement. EMBO J 25:1559-68.

471   12.   Yoder JD, Trask SD, Vo TP, Binka M, Feng N, Harrison SC, Greenberg HB, Dormitzer PR.
472   2009. VP5* rearranges when rotavirus uncoats. J Virol 83:11372-7.
473   13.   Trask SD, McDonald SM, Patton JT. 2012. Structural insights into the coupling of virion
474   assembly and rotavirus replication. Nat Rev Microbiol 10:165-77.
475   14.   Arias CF, Romero P, Alvarez V, López S. 1996. Trypsin activation pathway of rotavirus
476   infectivity. J Virol 70:5832-9.
477   15.   Gilbert JM, Greenberg HB. 1998. Cleavage of rhesus rotavirus VP4 after arginine 247 is
478   essential for rotavirus-like particle-induced fusion from without. J Virol 72:5323-7.
479   16.   Dormitzer PR, Nason EB, Prasad BV, Harrison SC. 2004. Structural rearrangements in the
480   membrane penetration protein of a non-enveloped virus. Nature 430:1053-8.
481   17.   Dormitzer PR, Sun ZY, Wagner G, Harrison SC. 2002. The rhesus rotavirus VP4 sialic acid
482   binding domain has a galectin fold with a novel carbohydrate binding site. EMBO J 21:885-
483   97.
484   18.   Fiore L, Greenberg HB, Mackow ER. 1991. The VP8 fragment of VP4 is the rhesus
485   rotavirus hemagglutinin. Virology 181:553-63.
486   19.   Graham KL, Halasz P, Tan Y, Hewish MJ, Takada Y, Mackow ER, Robinson MK, Coulson
487   BS. 2003. Integrin-using rotaviruses bind alpha2beta1 integrin alpha2 I domain via VP4
488   DGE sequence and recognize alphaXbeta2 and alphaVbeta3 by using VP7 during cell entry.
489   J Virol 77:9969-78.
490   20.   Graham KL, Takada Y, Coulson BS. 2006. Rotavirus spike protein VP5* binds alpha2beta1
491   integrin on the cell surface and competes with virus for cell binding and infectivity. J Gen
492   Virol 87:1275-1283.
493   21.   Estes MK, Graham DY, Gerba CP, Smith EM. 1979. Simian rotavirus SA11 replication in
494   cell cultures. J Virol 31:810-5.
495   22.   Enouf V, Chwetzoff S, Trugnan G, Cohen J. 2003. Interactions of rotavirus VP4 spike
496   protein with the endosomal protein Rab5 and the prenylated Rab acceptor PRA1. J Virol
497   77:7041-7.
498   23.   Zárate S, Cuadras MA, Espinosa R, Romero P, Juárez KO, Camacho-Nuez M, Arias CF,
499   López S. 2003. Interaction of rotaviruses with Hsc70 during cell entry is mediated by VP5. J
500   Virol 77:7254-60.
501   24.   Guerrero CA, Bouyssounade D, Zárate S, Isa P, López T, Espinosa R, Romero P, Méndez E,
502   López S, Arias CF. 2002. Heat shock cognate protein 70 is involved in rotavirus cell entry. J
503   Virol 76:4096-102.
504   25.   Li B, Ding S, Feng N, Mooney N, Ooi YS, Ren L, Diep J, Kelly MR, Yasukawa LL, Patton
505   JT, Yamazaki H, Shirao T, Jackson PK, Greenberg HB. 2017. Drebrin restricts rotavirus
506   entry by inhibiting dynamin-mediated endocytosis. Proc Natl Acad Sci U S A 114:E3642-
507   E3651.
508   26.   Nejmeddine M, Trugnan G, Sapin C, Kohli E, Svensson L, Lopez S, Cohen J. 2000.
509   Rotavirus spike protein VP4 is present at the plasma membrane and is associated with
510   microtubules in infected cells. J Virol 74:3313-20.
511   27.   Trejo-Cerro Ó, Eichwald C, Schraner EM, Silva-Ayala D, López S, Arias CF. 2018. Actin-
512   dependent nonlytic rotavirus exit and infectious virus morphogenetic pathway in
513   nonpolarized Cells. J Virol 92:e02076-17.
514   28.   Condemine W, Eguether T, Couroussé N, Etchebest C, Gardet A, Trugnan G, Chwetzoff S.
515   2019. The C terminus of rotavirus VP4 protein contains an actin binding domain which
516   requires cooperation with the coiled-coil domain for actin remodeling. J Virol 93:e01598-
517   18.
518   29.   Gardet A, Breton M, Fontanges P, Trugnan G, Chwetzoff S. 2006. Rotavirus spike protein
519   VP4 binds to and remodels actin bundles of the epithelial brush border into actin bodies. J
520   Virol 80:3947-56.

30. Gardet A, Breton M, Trugnan G, Chwetzoff S. 2007. Role for actin in the polarized release of rotavirus. J Virol 81:4892-4.

31. Wolf M, Vo PT, Greenberg HB. 2011. Rhesus rotavirus entry into a polarized epithelium is endocytosis dependent and involves sequential VP4 conformational changes. J Virol 85:2492-503.

32. Beckett D, Kovaleva E, Schatz PJ. 1999. A minimal peptide substrate in biotin holoenzyme synthetase-catalyzed biotinylation. Protein Sci 8:921-9.

33. De Lorenzo G, Eichwald C, Schraner EM, Nicolin V, Bortul R, Mano M, Burrone OR, Arnoldi F. 2012. Production of *in vivo*-biotinylated rotavirus particles. J Gen Virol 93:1474-82.

34. Predonzani A, Arnoldi F, López-Requena A, Burrone OR. 2008. *In vivo* site-specific biotinylation of proteins within the secretory pathway using a single vector system. BMC Biotechnol 8:41.

35. Fairhead M, Howarth M. 2015. Site-specific biotinylation of purified proteins using BirA. Methods Mol Biol 1266:171-84.

36. Roux KJ, Kim DI, Burke B. 2013. BioID: a screen for protein-protein interactions. Curr Protoc Protein Sci 74:19.23.1-19.23.14.

37. Fuerst TR, Niles EG, Studier FW, Moss B. 1986. Eukaryotic transient-expression system based on recombinant vaccinia virus that synthesizes bacteriophage T7 RNA polymerase. Proc Natl Acad Sci U S A 83:8122-6.

38. Kanai Y, Komoto S, Kawagishi T, Nouda R, Nagasawa N, Onishi M, Matsuura Y, Taniguchi K, Kobayashi T. 2017. Entirely plasmid-based reverse genetics system for rotaviruses. Proc Natl Acad Sci U S A 114:2349-2354.

39. Komoto S, Kanai Y, Fukuda S, Kugita M, Kawagishi T, Ito N, Sugiyama M, Matsuura Y, Kobayashi T, Taniguchi K. 2017. Reverse genetics system demonstrates that rotavirus nonstructural protein NSP6 is not essential for viral replication in cell culture. J Virol 91:e00695-17.

40. Papa G, Venditti L, Arnoldi F, Schraner EM, Potgieter C, Borodavka A, Eichwald C, Burrone OR. 2019. Recombinant rotaviruses rescued by reverse genetics reveal the role of NSP5 hyperphosphorylation in the assembly of viral factories. J Virol 94:e01110-19.

41. Papa G, Venditti L, Braga L, Schneider E, Giacca M, Petris G, Burrone OR. 2020. CRISPR-Csy4-mediated editing of rotavirus double-stranded RNA genome. Cell Rep 32:108205.

42. Jiménez-Zaragoza M, Yubero MP, Martín-Forero E, Castón JR, Reguera D, Luque D, de Pablo PJ, Rodríguez JM. 2018. Biophysical properties of single rotavirus particles account for the functions of protein shells in a multilayered virus. Elife 7:e37295.

43. Dormitzer PR, Greenberg HB, Harrison SC. 2000. Purified recombinant rotavirus VP7 forms soluble, calcium-dependent trimers. Virology 277:420-8.

44. Shaw RD, Vo PT, Offit PA, Coulson BS, Greenberg HB. 1986. Antigenic mapping of the surface proteins of rhesus rotavirus. Virology 155:434-51.

45. Eichwald C, Arnoldi F, Laimbacher AS, Schraner EM, Fraefel C, Wild P, Burrone OR, Ackermann M. 2012. Rotavirus viroplasm fusion and perinuclear localization are dynamic processes requiring stabilized microtubules. PLoS One 7:e47947.

46. Eichwald C, Rodriguez JF, Burrone OR. 2004. Characterization of rotavirus NSP2/NSP5 interactions and the dynamics of viroplasm formation. J Gen Virol 85:625-34.

47. Eichwald C, De Lorenzo G, Schraner EM, Papa G, Bollati M, Swuec P, de Rosa M, Milani M, Mastrangelo E, Ackermann M, Burrone OR, Arnoldi F. 2018. Identification of a small molecule that compromises the structural integrity of viroplasms and rotavirus double-layered particles. J Virol 92:e01943-17.

48. Kroschwald S, Alberti S. 2017. Gel or die: phase separation as a survival strategy. Cell 168:947-948.

571   49.   Lin Y, Mori E, Kato M, Xiang S, Wu L, Kwon I, McKnight SL. 2016. Toxic PR poly-
572   dipeptides encoded by the C9orf72 repeat expansion target LC domain polymers. Cell
573   167:789-802.e12.
574   50.   Geiger F, Papa G, Arter WE, Acker J, Saar KL, Erkamp N, Qi R, Bravo J, Strauss S,
575   Krainer G, Burrone OR, Jungmann R, Knowles TPJ, Engelke H, Borodavka A. Rotavirus
576   replication factories are complex ribonucleoprotein condensates. bioRxiv
577   https://doi.org/10.1101/2020.12.18.423429
578   51.   Déctor MA, Romero P, López S, Arias CF. 2002. Rotavirus gene silencing by small
579   interfering RNAs. EMBO Rep 3:1175-80.
580   52.   Trask SD, Dormitzer PR. 2006. Assembly of highly infectious rotavirus particles recoated
581   with recombinant outer capsid proteins. J Virol 80:11293-304.
582   53.   Herrmann T, Torres R, Salgado EN, Berciu C, Stoddard D, Nicastro D, Jenni S, Harrison
583   SC. 2021. Functional refolding of the penetration protein on a non-enveloped virus. Nature
584   590:666-670.
585   54.   Abdelhakim AH, Salgado EN, Fu X, Pasham M, Nicastro D, Kirchhausen T, Harrison SC.
586   2014. Structural correlates of rotavirus cell entry. PLoS Pathog 10:e1004355.
587   55.   Salgado EN, Garcia Rodriguez B, Narayanaswamy N, Krishnan Y, Harrison SC. 2018.
588   Visualization of calcium ion loss from rotavirus during cell entry. J Virol 92:e01327-18.
589   56.   Salgado EN, Upadhyayula S, Harrison SC. 2017. Single-particle detection of transcription
590   following rotavirus entry. J Virol 91: e00651-17.
591   57.   Trask SD, Kim IS, Harrison SC, Dormitzer PR. 2010. A rotavirus spike protein
592   conformational intermediate binds lipid bilayers. J Virol 84:1764-70.
593   58.   Vesikari T, Clark HF, Offit PA, Dallas MJ, DiStefano DJ, Goveia MG, Ward RL, Schödel
594   F, Karvonen A, Drummond JE, DiNubile MJ, Heaton PM. 2006. Effects of the potency and
595   composition of the multivalent human-bovine (WC3) reassortant rotavirus vaccine on
596   efficacy, safety and immunogenicity in healthy infants. Vaccine 24:4821-9.
597   59.   Ruiz-Palacios GM, Pérez-Schael I, Velázquez FR, Abate H, Breuer T, Clemens SC,
598   Cheuvart B, Espinoza F, Gillard P, Innis BL, Cervantes Y, Linhares AC, López P, Macías-
599   Parra M, Ortega-Barría E, Richardson V, Rivera-Medina DM, Rivera L, Salinas B, Pavía-
600   Ruz N, Salmerón J, Rüttimann R, Tinoco JC, Rubio P, Nuñez E, Guerrero ML, Yarzábal JP,
601   Damaso S, Tornieporth N, Sáez-Llorens X, Vergara RF, Vesikari T, Bouckenooghe A,
602   Clemens R, De Vos B, O'Ryan M, Group HRVS. 2006. Safety and efficacy of an attenuated
603   vaccine against severe rotavirus gastroenteritis. N Engl J Med 354:11-22.
604   60.   Ito N, Takayama-Ito M, Yamada K, Hosokawa J, Sugiyama M, Minamoto N. 2003.
605   Improved recovery of rabies virus from cloned cDNA using a vaccinia virus-free reverse
606   genetics system. Microbiol Immunol 47:613-7.
607   61.   Guglielmi KM, McDonald SM, Patton JT. 2010. Mechanism of intraparticle synthesis of the
608   rotavirus double-stranded RNA genome. J Biol Chem 285:18123-8.
609   62.   Arnold M, Patton JT, McDonald SM. 2009. Culturing, storage, and quantification of
610   rotaviruses. Curr Protoc Microbiol Chapter 15:Unit 15C.3.
611   63.   Yusa K, Zhou L, Li MA, Bradley A, Craig NL. 2011. A hyperactive piggyBac transposase
612   for mammalian applications. Proc Natl Acad Sci U S A 108:1531-6.
613   64.   Eichwald C, Vascotto F, Fabbretti E, Burrone OR. 2002. Rotavirus NSP5: mapping
614   phosphorylation sites and kinase activation and viroplasm localization domains. J Virol
615   76:3461-70.
616   65.   Sun M, Giambiagi S, Burrone O. 1997. [VP4 protein of simian rotavirus strain SA11
617   expressed by a baculovirus recombinant]. Zhongguo Yi Xue Ke Xue Yuan Xue Bao 19:48-
618   53.
619   66.   Arnoldi F, Campagna M, Eichwald C, Desselberger U, Burrone OR. 2007. Interaction of
620   rotavirus polymerase VP1 with nonstructural protein NSP5 is stronger than that with NSP2.
621   J Virol 81:2128-37.

622 67. Buttafuoco A, Michaelsen K, Tobler K, Ackermann M, Fraefel C, Eichwald C. 2020.
623   Conserved Rotavirus NSP5 and VP2 Domains Interact and Affect Viroplasm. J Virol 94.
624 68. Schindelin J, Arganda-Carreras I, Frise E, Kaynig V, Longair M, Pietzsch T, Preibisch S,
625   Rueden C, Saalfeld S, Schmid B, Tinevez JY, White DJ, Hartenstein V, Eliceiri K,
626   Tomancak P, Cardona A. 2012. Fiji: an open-source platform for biological-image analysis.
627   Nat Methods 9:676-82.
628 69. Eichwald C, Ackermann M, Nibert ML. 2018. The dynamics of both filamentous and
629   globular mammalian reovirus viral factories rely on the microtubule network. Virology
630   518:77-86.
631 70. Eichwald C, Ackermann M, Fraefel C. 2020. Mammalian orthoreovirus core protein μ2
632   reorganizes host microtubule-organizing center components. Virology 549:13-24.
633 71. Glück S, Buttafuoco A, Meier AF, Arnoldi F, Vogt B, Schraner EM, Ackermann M,
634   Eichwald C. 2017. Rotavirus replication is correlated with S/G2 interphase arrest of the host
635   cell cycle. PLoS One 12:e0179607.
636 72. Bauer M, Smith GP. 1988. Filamentous phage morphogenetic signal sequence and
637   orientation of DNA in the virion and gene-V protein complex. Virology 167:166-75.
638

639 **FIGURE LEGENDS**

640 **Figure 1. Generation of VP4-BAP tagged recombinant rotavirus (A)** Schematic representation

641 of BAP tag inserted in lectin domain loops of the VP8* subunit of VP4 from RV simian strain

642 SA11(GenBank: X14204.1). The lysine (K, red) indicates the biotinylation site by BirA ligase. Four

643 different VP4 proteins tagged with BAP (VP4-BAP) were built between amino acid regions T96-

644 R101 (blue), E109-S114(orange), N132-Q137 (pink), and K145-G150 (green). VP4 trimer ribbon

645 structure for visualization of VP5CT (body and stalk, red) and VP8* (yellow) fragments. An inset

646 in VP8* indicates the different positions in hydrophobic loops of VP8* where the inserted BAP tags

647 were colored in blue, orange, pink, and green. **(B)** Western blot retardation assay of cell lysates

648 transiently expressing wtVP4 and VP4-BAP tagged at blue, orange, pink, and green positions,

649 respectively. Untreated (-) and treated (+) samples with streptavidin are indicated. Immunoblot was

650 incubated with anti-VP4 to detect unbound and bound VP4 to streptavidin (VP4-BAP•StAv).

651 Alpha-tubulin was used as a loading control**. (C)** Comparison of the dsRNA genome segments

652 migration pattern of rRV/wt and rRV/VP4-BAP. The red arrow points to gs -BAP. **(D)** Virus

653 replication fitness curve between 0 to 48 hpi of rRV/wt and rRV/VP4-BAP. **(E)** Immunoblotting of

654 uninfected (-) or infected cell lysates in MA-cytBirA (left panel) or MA104 (right panel) with

655   rRV/wt or rRV/VP4-BAP [MOI, 25 VFU/cell]. Biotinylated proteins were detected with StAv-

656   HRP. Alpha-tubulin was used as a loading control. The red star and red arrow indicate biotinylated

657   VP4-BAP and host undetermined biotinylated protein, respectively. **(F)** WB-ra of MA-cytBirA cell

658   lysates infected with rRV/wt or rRV/VP4-BAP untreated or treated with StAv. The membrane was

659   incubated with anti-VP4 and anti-VP6 for the detection of virus proteins. Alpha-tubulin was used as

660   a loading control. The percentage of biotinylated VP4 normalized according to VP6 expression is

661   indicated. **(G)** WB-ra of purified rRV/VP4-BAP particles incubated without (-) and with (+)

662   streptavidin. The membrane was incubated for the detection of VP4-BAP (anti-VP4) and VP6 (anti-

663   VP6). Alpha-tubulin was used as a loading control. The percentage of biotinylated VP4-BAP was

664   determined and normalized to the expression of VP6. **(H)** Visualization at a high resolution of

665   purified virions isolated of rRV/VP4-BAP infected MA-cytBirA cells untreated (-biotin, upper

666   panel) or treated (+biotin, lower panel) with 100µM biotin. After purification, the virions were

667   labeled with streptavidin conjugated to colloidal gold (12 nm), followed by negative staining and

668   visualization at the electron microscope (right panel). Scale bar is 100 nm

669   **Figure 2. virus entry and RV protein localization upon rRV/VP4-BAP infection. (A)**

670   Internalization in MA104 cells of purified virions at 0 min (upper panel) and 2 min (lower panel).

671   Purified virions of rRV/wt and biotinylated rRV/VP4-BAP were previously labeled with StAv-

672   Alexa 555 (red). At the indicated time points, cells were fixed and immunostained for VP7 trimers

673   detection (mAb anti-VP7 clone 159, pink) and MTs (anti- α-tubulin, green). Nuclei were stained

674   with DAPI (blue). White open boxes indicate the magnified images at the right. Arrows point to

675   virus particle clamps detected with VP7. Scale bar is 20 µm. **(B)** MA-cytBirA cells infected with

676   rRV/wt (top panel) and rRV/VP4-BAP (bottom panel) untreated (-biotin) and treated (+biotin) with

677   biotin. Cells were PFA fixed at 6 hpi and stained for viroplasms (anti-NSP5, green) and biotinylated

678   proteins (streptavidin-Alexa 555, red) detection. Nuclei were stained with DAPI (blue). **(C)**

679   Immunostaining images of rRV/VP4-BAP infected MA-cytBirA cells in the presence of biotin. At

680   6 hpi, PFA fixed cells were stained for the detection of VP4-BAP (StAv, red) with viroplasms (anti-

681 NSP5, green) (left row) or mature RV particles (anti-VP7 clone 159, green) (right row). **(D)**

682 immunofluorescence images comparing localization of VP4 and VP4-BAP (anti-VP4, red) of cells

683 infected with rRV/wt (left row) or rRV/VP4-BAP (right row). Viroplasms were detected with anti-

684 NSP5 (green). The dashed white boxes correspond to the image insets of the right columns. Purple

685 arrows point to the VP4-BAP streptavidin signal. Scale bar is 10 μm.

686 **Figure 3. rRV/VP4-BAP viroplasms revealed a delayed dynamic associated with VP4 role. (A)**

687 Schematic representation for the characterization of LLPS condensates on viroplasms of rRV/VP4-

688 BAP-infected cells. At 5 hpi, RV infected MA/NSP2-mCherry cells were treated with 1,6-HD for 6

689 min. The drug was washed out, and samples were fixed and imaged for viroplasm quantification at

690 0-, 2-, 15- and 30-min post-recovery. **(B)** 1,6-HD recovery plot of cells showing viroplasms

691 normalized to initial conditions (5 hpi). **(C)** 1,6-HD recovery plot of viroplasm counts per cell upon

692 infection with rRV/VP4-BAP (green column) and rRV/wt (grey column). Plots of viroplasm counts

693 per cell **(D)** and viroplasm size per cell **(E)** at initial conditions (5 hpi). **(F)** 1,6-HD recovery plot of

694 normalized viroplasm size at initial conditions. **(G)** FRAP recovery curve of NSP2-mCherry of

695 single viroplasms of rRV/VP4-BAP (green) and rRV/wt (grey) infected MA/NSP2-mCherry cells, 5

696 hpi (n=27 and 25, respectively). 1,6-HD recovery plots showing appearing viroplasms **(H)**, number

697 of viroplasms per cell **(I),** and viroplasm size per cell **(J)** of SA11 infected MA104 cells silenced

698 with siVP4 (orange) or control siRNA (scr, blue). Data represent mean ± SEM Student's t-test (*),

699 p<0.05; (**), p<0.01 and (***), p<0.001

700

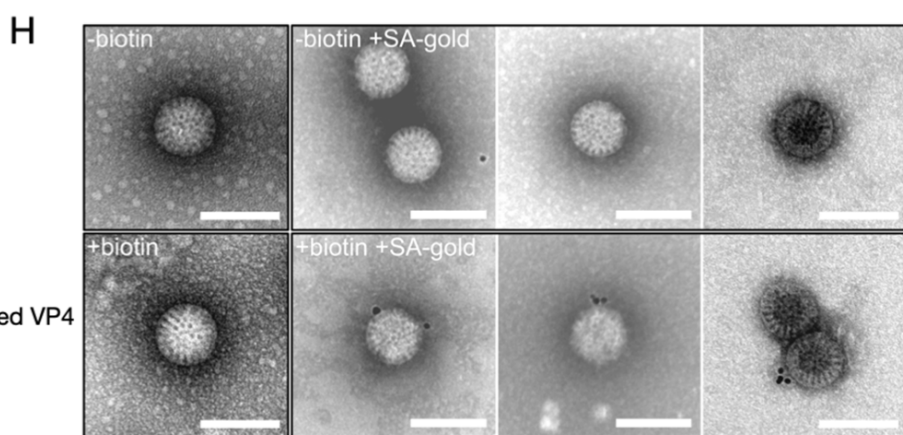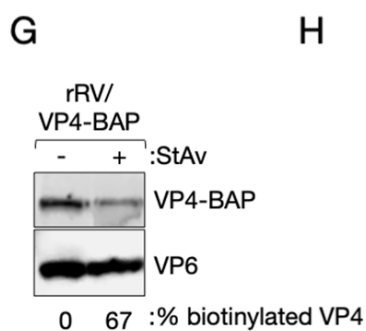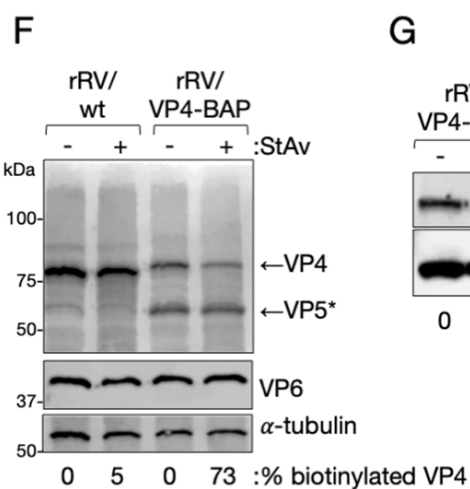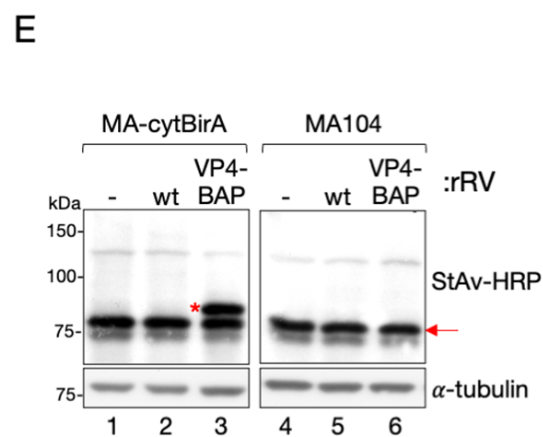701 **SUPPLEMENTAL MATERIAL**

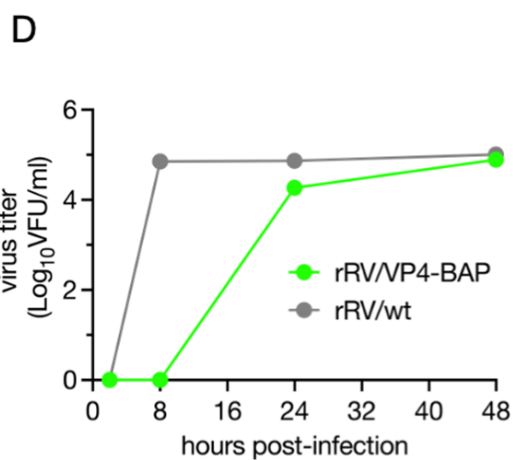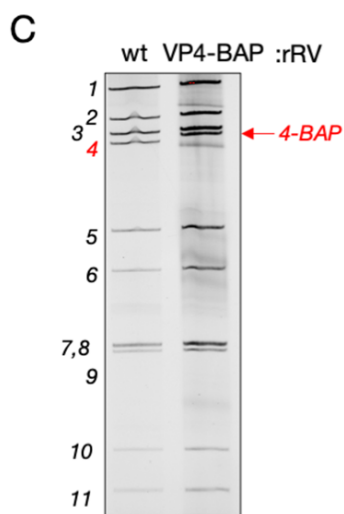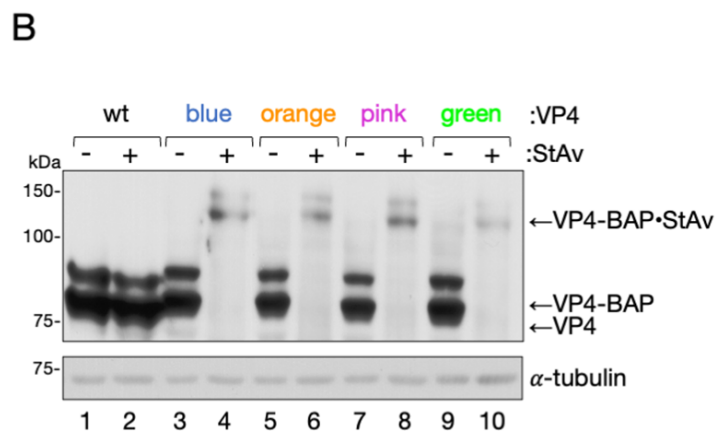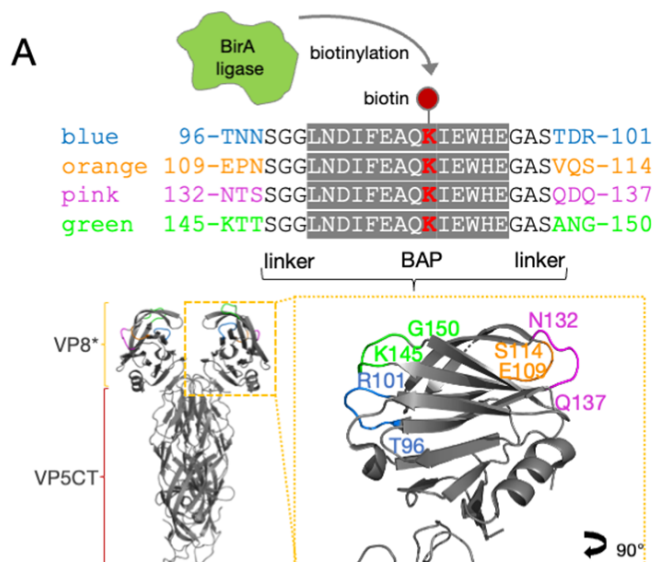702 **SUPPLEMENTARY FIGURE LEGENDS**

703 **Figure S1. (A)** Immunoblotting of cellular extracts of transfected VP4-BAP (lane 1) and infected

704 rRV/VP4-BAP (lane 2). **(B)** Immunoblot of cellular extracts of transfected VP4-BAP untreated (-)

705 or treated (+) with lambda phosphatase. VP4-BAP shifted band is indicated with a red start.
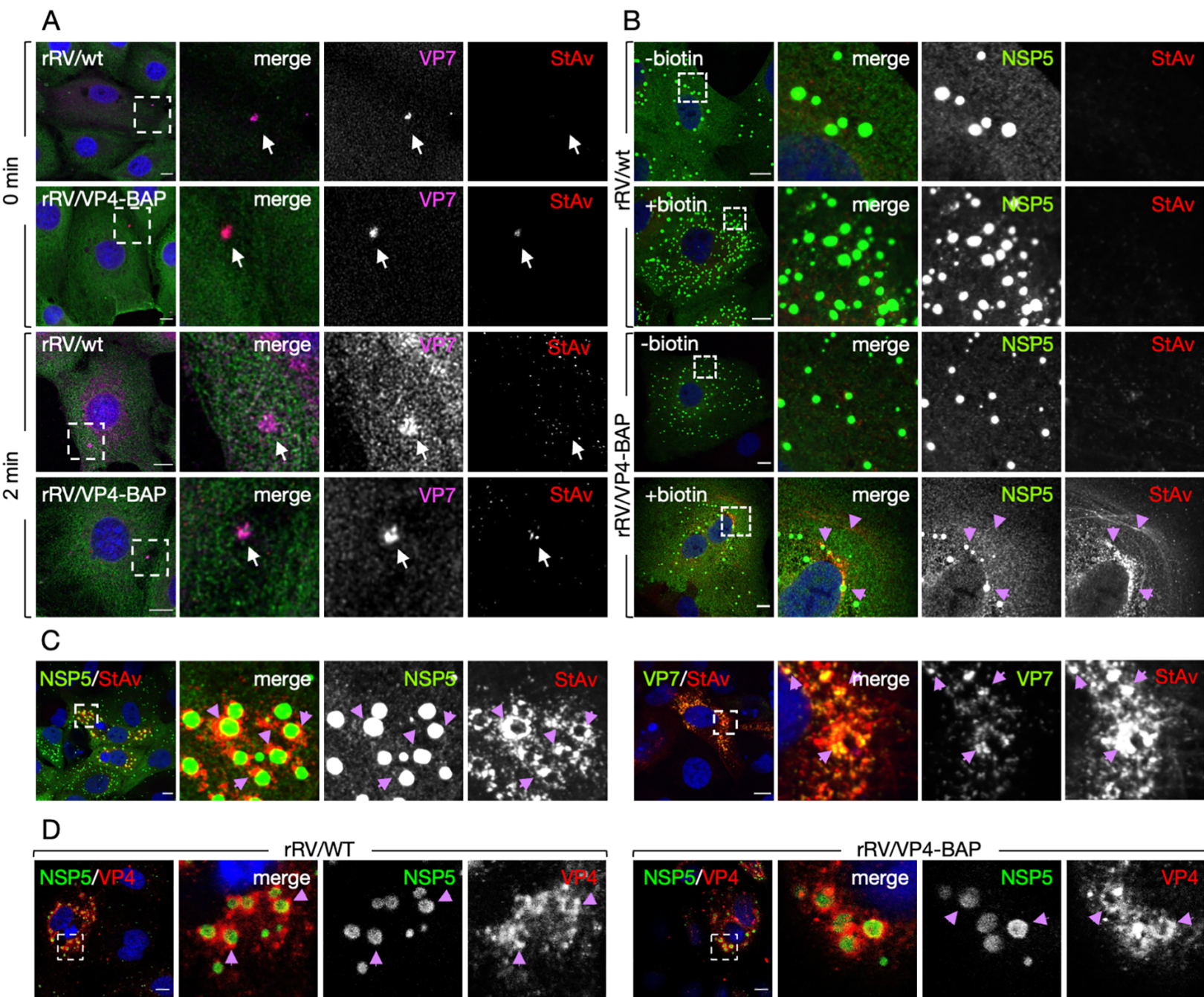
706   Membranes were incubated with anti-VP4 and anti-tubulin. **(C)** Sequence chromatogram of gs4-

707   BAP of rRV/VP4-BAP visualizing inserted linkers and BAP tag. Nucleotide (top) and amino acid

708   (bottom) sequences are indicated. **(D)** Negative staining of virion layers detected in purified

709   rRV/VP4-BAP preparations. The yellow arrow points to TLPs. Scale bar is 100 nm. **(E)** Scatter dot

710   plot comparing the diameter of purified particles from non-biotinylated (-biotin, light green) or

711   biotinylated (+biotin, dark green) RV/VP4-BAP and rRV/wt (grey). The median value is indicated,
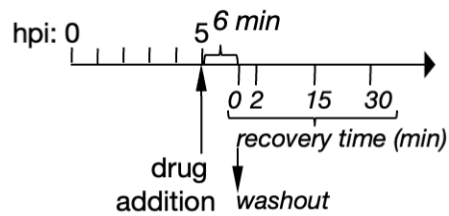
712   n>40 particles, t-test student, (*) p-value<0.05.
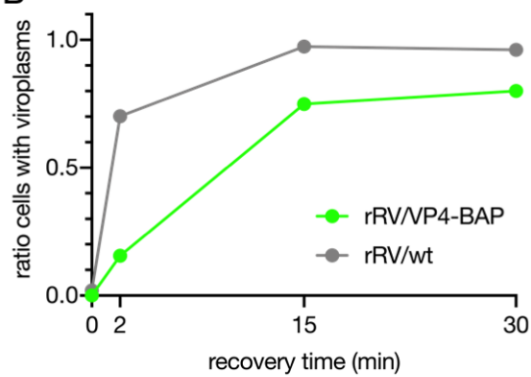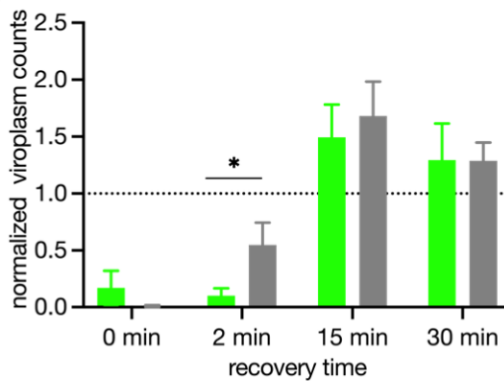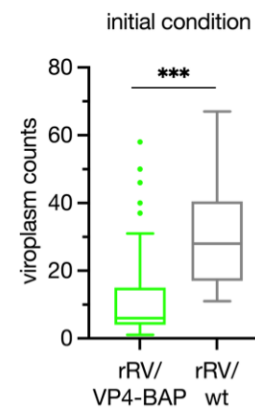
713   **Figure S2. (A)** Immunofluorescence images of viroplasms (anti-NSP5, green) from cells infected

714   with rRV/wt (left panel) or rRV/VP4-BAP (right panel). At 6 hpi, cells were fixed with either PFA

715   (upper row) or methanol (lower row), followed by immunostaining. Nuclei were stained with DAPI

716   (blue). White arrowheads point to green aggregates. Scale bar is 20 μm. **(B)** Representative images

717   of MA-NSP2-mCherry cells infected at 5 hpi with rRV/wt (upper row) or rRV/VP4-BAP (lower

718   row) and treated for 6 min with 3.5% of 1,6-HD. Cells were washed and monitored for viroplasm

719   formation at 0-, 2-, 15- and 30-min post-recovery. White arrows point to cells showing recovered
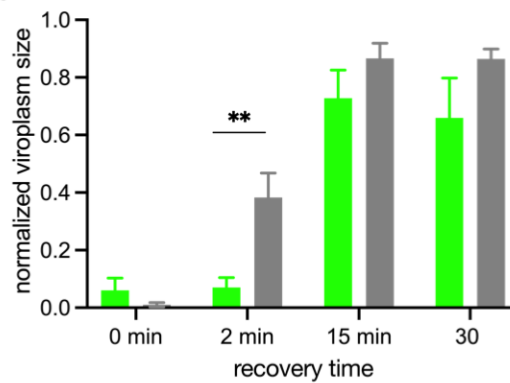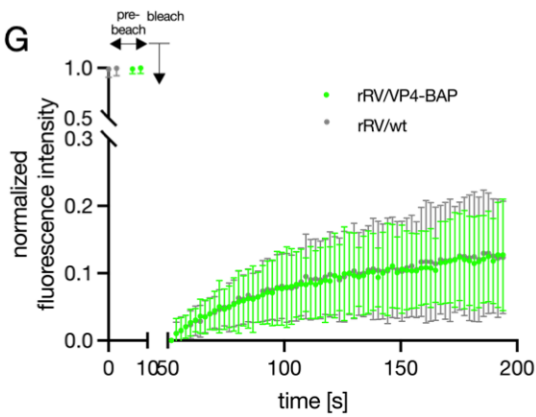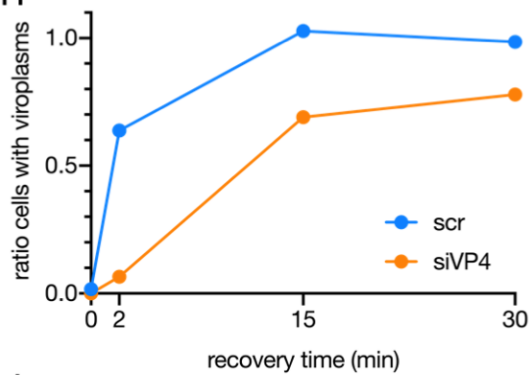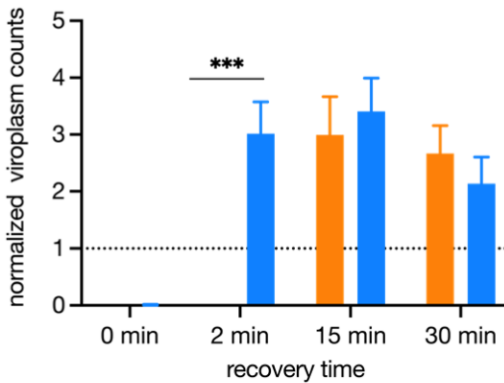
720   viroplasms. Scale bar is 10 μm. **(C)** Plot for the perinuclear ratio of cells infected with rRV/VP4-

721   BAP and rRV/wt at initial conditions (5 hpi). **(D)** 1,6-HD recovery plot of the normalized

722   perinuclear ratio of viroplasms from cells infected with rRV/VP4-BAP (green) and rRV/wt (grey).

723   **(E)** Fluorescence images of FRAP measurement of single viroplasms of cells infected with

724   rRV/VP4 (top) and rRV/wt (bottom) at pre-bleach, post-bleach, and recovery time conditions. Each

725   inset indicates the bleached viroplasm of the images at the right. Nuclei were stained with Hoescht

726   33342. Scale bar is 10 μm. Plots of the T-half recovery **(F)** and the mobile fraction **(G)** means of

727   single viroplasms of rRV/VP4-BAP and rRV/wt.

728   **Figure S3. (A)** Immunoblot of 6 hpi cellular lysates prepared from MA104 or MA-NSP2-mCherry

729   cells silenced with siVP4 or control siRNA (scr) followed by mock-infection or infection with RV

730   simian strain SA11. The membrane was stained with anti-VP4, anti-NSP5, and anti-GAPDH

731   (loading control). **(B)** Immunostaining at 6 hpi of SA11-infected MA-NSP2-mCherry cells knocked

732   down with control siRNA (scr) (upper row) or siVP4 (lower row). Cells were immunostained with

733   anti-VP4 (green). Nuclei were stained with DAPI (blue). Scale bar is 10 μm. **(C)**

734   Immunofluorescence analysis at 6 hpi of SA11-infected MA104 cells silenced with siVP4 or

735   control siRNA. Cells were fixed either PFA (upper row) or methanol (lower row), followed by

736   viroplasm immunostaining (anti-NSP5, green). Nuclei were stained with DAPI (blue). White

737   arrowheads point to diffuse viroplasms. Scale bar is 20 μm. **(D)** Representative images of SA11-

738   infected MA-NSP2-mCherry cells knocked down with scr (upper row) or siVP4 (lower row) and

739   treated for 6 min with 3.5% of 1,6-HD. Cells were washed and monitored for viroplasm formation

740   at 0-, 2-, 15- and 30-min post-recovery. White arrows point to cells showing recovered viroplasms.

741   Scale bar is 10 μm.

742

A

BirA ligase → biotinylation → biotin

blue   96-TNNSGG**LNDIFEAQKIEWHE**GAS TDR-101
orange 109-EPNSGG**LNDIFEAQKIEWHE**GAS VQS-114
pink   132-NTSSGG**LNDIFEAQKIEWHE**GAS QDQ-137
green   145-KTTSGG**LNDIFEAQKIEWHE**GAS ANG-150

linker   BAP   linker

VP8*
VP5CT

G150   N132
K145   S114
R101   E109
T96   Q137

90°

B

	wt		blue		orange		pink		green		:VP4

kDa   - +   - +   - +   - +   - +   :StAv

150 —
100 —   ← VP4-BAP•StAv
75 —   ← VP4-BAP
                                         ← VP4

75 —   α-tubulin

1 2   3 4   5 6   7 8   9 10

C

wt VP4-BAP :rRV

1
2
3
4   ← 4-BAP
5
6
7,8
9
10
11

D

virus titer (Log₁₀VFU/ml) vs hours post-infection

● rRV/VP4-BAP
● rRV/wt

E

	MA-cytBirA			MA104			

kDa   - wt VP4-BAP   - wt VP4-BAP :rRV

150 —
100 —   StAv-HRP
75 —   *   ←

75 —   α-tubulin

1   2   3   4   5   6

F

	rRV/wt		rRV/VP4-BAP	

kDa   - +   - +   :StAv

100 —
75 —   ← VP4
                    ← VP5*
50 —
37 —   VP6
50 —   α-tubulin

0   5   0   73 :% biotinylated VP4

G

rRV/VP4-BAP
- + :StAv

VP4-BAP
VP6

0   67 :% biotinylated VP4

H

-biotin   -biotin +SA-gold
+biotin   +biotin +SA-gold